



Circular Nonlinear Subdivision Schemes for Curve Design

Jian-ao Lian[§], Yonghui Wang[†], & Yonggao Yang[‡]

Department of {Mathematics[§], Engineering Technology[†], Computer Science[‡]}
Prairie View A&M University
Prairie View, TX 77446-0519 USA
[jilian, yowang, yoyang}@pvamu.edu](mailto:{jilian, yowang, yoyang}@pvamu.edu)

Received: March 25, 2009; Accepted: June 8, 2009

Abstract

Two new families of *nonlinear* 3-point subdivision schemes for curve design are introduced. The first family is ternary interpolatory and the second family is binary approximation. All these new schemes are *circular-invariant*, meaning that new vertices are generated from local circles formed by three consecutive old vertices. As consequences of the nonlinear schemes, two new families of *linear* subdivision schemes for curve design are established. The 3-point *linear* binary schemes, which are corner-cutting depending on the choices of the tension parameter, are natural extensions of the Lane-Riesenfeld schemes. The four families of both nonlinear and linear subdivision schemes are implemented extensively by a variety of examples.

Keywords: Subdivision; Curve design; Computer-aided geometric design; Refinable functions

MSC (2000) No.: 14H50; 65D17; 68U07

1. Introduction

THE well-known family of 2-point corner-cutting subdivision schemes for curve design was given by

$$\begin{aligned}\lambda_{2k}^{(n+1)} &= (1-w)\lambda_k^{(n)} + w\lambda_{k+1}^{(n)}, \\ \lambda_{2k+1}^{(n+1)} &= w\lambda_k^{(n)} + (1-w)\lambda_{k+1}^{(n)}, \quad k \in \mathbb{Z}; \quad n \in \mathbb{Z}_+, \end{aligned} \quad (1)$$

with $\lambda_k^{(0)}$, $k \in \mathbb{Z}$, being the initial vertices of the 2D or 3D polygonal curve, where, for each natural

number n , $\lambda_k^{(n)}$, $k \in \mathbb{Z}$, are the n^{th} level vertices, $\lambda_k^{(n+1)}$'s are the $(n+1)^{\text{st}}$ level vertices, and w is a tension parameter on $(0, 1/2)$. The particular choice of $w = 1/4$ corresponds to the classical de Rham-Chaikin scheme (Rham [11] and Chaikin [1]). It has a simple geometric interpretation: Each line segment from $\lambda_k^{(n)}$ to $\lambda_{k+1}^{(n)}$, or $\lambda_{k+1}^{(n)} - \lambda_k^{(n)}$ in its vector form, is partitioned based on the ratio of $w:(1-2w):w$; and the two points $\lambda_k^{(n)} + w(\lambda_{k+1}^{(n)} - \lambda_k^{(n)})$ and $\lambda_{k+1}^{(n)} - w(\lambda_{k+1}^{(n)} - \lambda_k^{(n)})$, named as $\lambda_{2k}^{(n+1)}$ and $\lambda_{2k+1}^{(n+1)}$, respectively, will be two new vertices to form the next level polygon. The limiting curve has C^1 -continuity. More precisely, it is well-known that the de Rham-Chaikin scheme converges to a linear combination of integer shifts of the quadratic B -spline $N_3(t)$, given explicitly by

$$N_3(t) = \begin{cases} \frac{1}{2}t^2 & \text{if } t \in [0, 1), \\ \frac{3}{4} - \left(t - \frac{3}{2}\right)^2 & \text{if } t \in [1, 2), \\ \frac{1}{2}(3-t)^2 & \text{if } t \in [2, 3), \\ 0 & \text{otherwise.} \end{cases}$$

Scheme deduced from the de Rham-Chaikin scheme for surface design was consequently developed by (Doo & Sabin [4]).

The generic form (1) is also referred as the Lane-Riesenfeld (refine and smooth) scheme (Land & Riesenfeld [8]). The scheme (1) is linear, i.e., all current level vertices are generated by a *linear combination* of consecutive local vertices of the previous level's. It is an approximation scheme, which means that old vertices are *not explicitly kept* for the new level. However, it is not hard to verify that it is not *circular-invariant*, meaning, with the initial 2D polygon as cyclic polygons, the limiting curve of the subdivision scheme is not a circle. Here a cyclic polygon is a polygon that has a circumscribed circle, such as a square, a rectangle, or an isosceles trapezoid.

First of all, a circular-invariant subdivision scheme for curve design is in general nonlinear. Secondly, the study of subdivision schemes nowadays is closely related to the development of the *refinable functions* in wavelet theory. For instance, family of binary schemes can be induced from refinable functions with dilation 2 (Daubechies [3]), while family of ternary schemes are induced from refinable functions with dilation 3 (Chui & Lian [2]). As an example, the scheme in (1) can be induced from the refinable function ϕ satisfying

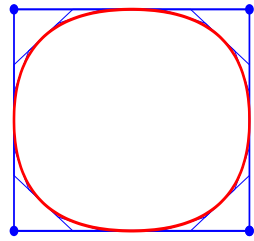
$$\phi(x) = w\phi(2x) + (1-w)\phi(2x-1) + (1-w)\phi(2x-2) + w\phi(2x-3). \quad (2)$$

With appropriate normalization conditions and up to a sign change, (2) determines a unique continuous function ϕ for any $w \in (0, 1)$. By taking the Fourier transform of (2) both sides, we arrive at the two-scale equation of ϕ :

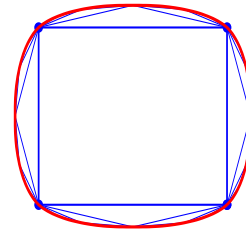
$$\widehat{\phi}(\omega) = P(e^{-i\omega/2}) \widehat{\phi}\left(\frac{\omega}{2}\right), \quad (3)$$

$$P(z) = \frac{1}{2}(w + (1-w)z + (1-w)z^2 + wz^3) = \frac{1+z}{2}(w + (1-2w)z + wz^2), \quad (4)$$

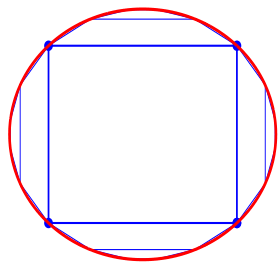
where $P(z)$ in (3)-(4) is called the *two-scale symbol* of ϕ . All properties of ϕ are now reflected on the two-scale symbol $P(z)$ in (4). Meanwhile, recall that the classical 4-point interpolatory



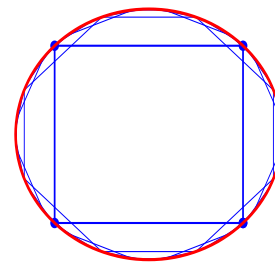
(a) Initial square & the 6th level subdivision by using the de Rham-Chaikin scheme.



(b) Initial square & the 6th level subdivision by using the 4-point scheme induced from the two-scale symbol P_4 in (5).



(c) Initial square & the 6th level subdivision by using our ternary interpolatory scheme (6) in Section 2.



(d) Initial square & the 6th level subdivision by using our binary approximation scheme (9) in Section 2.

Figure 1. Four different schemes are applied to an initial polygon as a unit square. The four schemes are the de Rham-Chaikin corner-cutting scheme, the classical 4-point scheme, our 3-point circular-invariant ternary interpolatory scheme, and our 3-point circular-invariant binary approximation scheme.

scheme for curve design, introduced in (Dyn, et al. [5]) and consequently studied by many other researchers (cf., e.g., Ivriissimtzisa, et al. [7] & Lian [9]), can be induced from a refinable function. If we denote by ϕ_4 the refinable function associated to the 4-point interpolatory scheme and satisfying (3) with two-scale symbol, denoted by P_4 , then P_4 is given explicitly by

$$P_4(z) = \frac{1}{2z^3} \left(-\frac{1}{16} + \frac{9}{16}z^2 + z^3 + \frac{9}{16}z^4 - \frac{1}{16}z^6 \right) = \frac{1}{2z^3} \left(\frac{1+z}{2} \right)^4 (-1 + 4z - z^2). \quad (5)$$

When both the corner-cutting scheme in (1) with $w = 1/4$ and the 4-point scheme induced from (2) are applied to the unit square, the results are shown in Fig. 1. The limiting curves in both Fig. 1(a) and Fig. 1(b) are not circles. On the other hand, by using our 3-point circular-invariant ternary interpolatory and binary approximation schemes described in Section 2, the limiting curves in both Fig. 1(c) and Fig. 1(d) are circles.

We point out that the 4-point interpolatory scheme was established way before the rapid development of wavelets. Not only is it interesting to observe the overlap among researchers in both CAD/CAGD/CAM and wavelet communities but it definitely triggers off innovative tools for

the smoothness analysis of subdivision schemes and stimulate research development of the two communities.

One of the main objectives of this paper is to introduce two new families of nonlinear 3-point subdivision schemes for curve design, both planar and 3D. The first family is *ternary interpolatory* while the second family is *binary approximation*. All these new schemes are circular-invariant, with the local three or two new vertices being generated from local circles formed by the three consecutive old vertices. Again, the schemes can be applied to both planar and 3D polygons.

Our main results are listed in Section 2. A brief analysis of convergence is provided in Section 3. Extensive demonstrations are included in Sections 4. Conclusions constitute Section 5.

2. Main Results

We establish two families of subdivision schemes. The first family is *ternary and interpolatory*, given by

$$\begin{aligned}\lambda_{3k-1}^{(n+1)} &= w\lambda_{k-1}^{(n)} + (1-w)\lambda_k^{(n)} + \alpha_k^{(n)}(\lambda_k^{(n)} - \lambda_{k+1}^{(n)}), \\ \lambda_{3k}^{(n+1)} &= \lambda_k^{(n)}, \\ \lambda_{3k+1}^{(n+1)} &= (1-w)\lambda_k^{(n)} + w\lambda_{k+1}^{(n)} + \beta_k^{(n)}(\lambda_k^{(n)} - \lambda_{k-1}^{(n)}),\end{aligned}\quad k \in \mathbb{Z}; \quad n \in \mathbb{Z}_+, \quad (6)$$

where both $\alpha_k^{(n)}$ and $\beta_k^{(n)}$ are so chosen that both $\lambda_{3k-1}^{(n+1)}$ and $\lambda_{3k+1}^{(n+1)}$ in (6) are two intersections of the circle formed by $\lambda_{k-1}^{(n)}$, $\lambda_k^{(n)}$, and $\lambda_{k+1}^{(n)}$; and w is a tension parameter on $(0, 1)$. See Fig.2 for a geometric illustration with $w = 2/9$.

Figure 2. The geometric illustration of the nonlinear 3-point ternary interpolatory subdivision scheme in (6) with $w = 2/9$. The two segments are partitioned based upon the ratio of 2:7, or $w:(1-w)$ in general, from the interpolatory vertex (marked blue). Then a new line is drawn from each partitioned point in such a way that the line is parallel to the other line segment. The intersections of the two new lines with the circle formed by the three vertices are the new vertices for the next level (marked solid and dark). Here the intersections are chosen to be outside of the triangle (formed by the three old vertices). The two gray dots are the new vertices generated from the linear ternary subdivision scheme. They are plotted here for reference only.

Observe that, first, both $\alpha_k^{(n)}$ and $\beta_k^{(n)}$ for each k depend on w and $\lambda_{k-1}^{(n)}$, $\lambda_k^{(n)}$, and $\lambda_{k+1}^{(n)}$. The

actual detailed expressions of $\alpha_k^{(n)}$ and $\beta_k^{(n)}$ in (6) are omitted here. Secondly, if we write

$$\alpha_k^{(n)} = \alpha_k^{(n)}(w, \lambda_{k-1}^{(n)}, \lambda_k^{(n)}, \lambda_{k+1}^{(n)}), \quad \beta_k^{(n)} = \beta_k^{(n)}(w, \lambda_{k-1}^{(n)}, \lambda_k^{(n)}, \lambda_{k+1}^{(n)}), \quad (7)$$

the symmetry of the scheme in (6) is guaranteed by the fact that

$$\alpha_k^{(n)}(w, \lambda_{k-1}^{(n)}, \lambda_k^{(n)}, \lambda_{k+1}^{(n)}) = \beta_k^{(n)}(w, \lambda_{k+1}^{(n)}, \lambda_k^{(n)}, \lambda_{k-1}^{(n)}), \quad (8)$$

simply due to the fact that the circle formed by $\lambda_{k-1}^{(n)}$, $\lambda_k^{(n)}$, and $\lambda_{k+1}^{(n)}$ is the same as that formed by $\lambda_{k+1}^{(n)}$, $\lambda_k^{(n)}$, and $\lambda_{k-1}^{(n)}$.

The second family is *binary approximation*, given by

$$\begin{aligned} \lambda_{2k-1}^{(n+1)} &= w\lambda_{k-1}^{(n)} + (1-w)\lambda_k^{(n)} + \alpha_k^{(n)}(\lambda_k^{(n)} - \lambda_{k+1}^{(n)}), \\ \lambda_{2k}^{(n+1)} &= (1-w)\lambda_k^{(n)} + w\lambda_{k+1}^{(n)} + \beta_k^{(n)}(\lambda_k^{(n)} - \lambda_{k-1}^{(n)}), \quad k \in \mathbb{Z}; \quad n \in \mathbb{Z}_+, \end{aligned} \quad (9)$$

with both $\alpha_k^{(n)}$ and $\beta_k^{(n)}$ being chosen in the same manner as in ternary interpolatory schemes, and w is, again, a tension parameter $\in (0, 1)$. We also point out that the schemes in (9) are indeed *corner-cutting*. Analogously, the symmetry of the schemes in (9) is reflected by (7)–(8).

Fig. 2 is also valid for illustration of the binary schemes in (9), but with the blue dot marked as open, i.e., not kept or not interpolated.

When both $\alpha_k^{(n)}$ and $\beta_k^{(n)}$ in (6) are depending only on the tension parameter w , say,

$$\alpha_k^{(n)} = \beta_k^{(n)} = \frac{1}{3} - w, \quad (10)$$

the schemes are linear. So, as consequences of (6), we have the following family of 3-point linear ternary interpolatory subdivision schemes

$$\begin{aligned} \lambda_{3k-1}^{(n+1)} &= w\lambda_{k-1}^{(n)} + \left(\frac{4}{3} - 2w\right)\lambda_k^{(n)} + \left(w - \frac{1}{3}\right)\lambda_{k+1}^{(n)}, \\ \lambda_{3k}^{(n+1)} &= \lambda_k^{(n)}, \\ \lambda_{3k+1}^{(n+1)} &= \left(w - \frac{1}{3}\right)\lambda_{k-1}^{(n)} + \left(\frac{4}{3} - 2w\right)\lambda_k^{(n)} + w\lambda_{k+1}^{(n)}, \quad k \in \mathbb{Z}; \quad n \in \mathbb{Z}_+, \end{aligned} \quad (11)$$

The choice of $w = 2/9$ is a linear stationary scheme, studied in (Hassan & Dodgson [6]) and is a special case in (Lian [10]). The choice of $w = 1/6$ makes the three new vertices collinear.

Analogously, when both $\alpha_k^{(n)}$ and $\beta_k^{(n)}$ in (9) are depending only on w , say,

$$\alpha_k^{(n)} = \beta_k^{(n)} = \frac{1}{4} - w, \quad (12)$$

the schemes are also linear. So, again, as consequences of (9), we arrive at the following family of 3-point corner-cutting, linear, and binary approximation subdivision schemes

$$\begin{aligned} \lambda_{2k-1}^{(n+1)} &= w\lambda_{k-1}^{(n)} + \left(\frac{5}{4} - 2w\right)\lambda_k^{(n)} + \left(w - \frac{1}{4}\right)\lambda_{k+1}^{(n)}, \\ \lambda_{2k}^{(n+1)} &= \left(w - \frac{1}{4}\right)\lambda_{k-1}^{(n)} + \left(\frac{5}{4} - 2w\right)\lambda_k^{(n)} + w\lambda_{k+1}^{(n)}, \quad k \in \mathbb{Z}; \quad n \in \mathbb{Z}_+. \end{aligned} \quad (13)$$

When $w = 1/4$, (13) becomes the de Rham-Chaikin scheme. So (13) is de facto a natural extension of the Lane-Riesenfeld schemes in (1). When $w = 1/8$, the three new vertices are collinear. These schemes converge to continuous curves when $w \in (-1/8, 7/8)$; in at least a C^1 fashion when $w \in (1/8, 5/8)$; at least C^2 when $w \in (1/4, 1/2)$; and C^4 only when $w = 5/16$ (quartic B -splines).

3. Brief Analysis of Convergence

To ensure the convergence of all new subdivision schemes in this paper, we provide a brief convergence analysis in this section without giving too many details.

There are two ways to study the limiting behavior of the two families of subdivision schemes in (6) and (9). First, observe that, considering $\lambda_k^{(n)}$'s as column vectors for each n , the schemes in (6) can be rewritten into the following matrix form

$$[\lambda_{3k-1}^{(n+1)}, \lambda_{3k}^{(n+1)}, \lambda_{3k+1}^{(n+1)}] = [\lambda_{k-1}^{(n)}, \lambda_k^{(n)}, \lambda_{k+1}^{(n)}] M_k^{(n)}, \quad (14)$$

where

$$M_k^{(n)} = \begin{bmatrix} w & 0 & -\beta_k^{(n)} \\ 1 - w + \alpha_k^{(n)} & 1 & 1 - w + \beta_k^{(n)} \\ -\alpha_k^{(n)} & 0 & w \end{bmatrix},$$

The convergence of the schemes in (6) can then be confirmed by analyzing the convergence of the product

$$\prod_{\ell=0}^n M_{3^\ell k}^{(\ell)} = M_k^{(0)} M_{3k}^{(1)} M_{3^2 k}^{(2)} \cdots M_{3^n k}^{(n)}$$

of the matrix sequence $\{M_{3^\ell k}^{(\ell)}\}_{\ell \in \mathbb{Z}_+}$. Another way is to check the behavior of the product of polynomials (or two-scale symbols) P , namely,

$$\prod_{\ell=0}^n P_{3^\ell k}^{(\ell)} \left(e^{-i\omega/3^{n+1-\ell}} \right) = P_{3^n k}^{(n)} \left(e^{-i\omega/3} \right) P_{3^{n-1} k}^{(n-1)} \left(e^{-i\omega/3^2} \right) P_{3k}^{(1)} \left(e^{-i\omega/3^n} \right) P_k^{(0)} \left(e^{-i\omega/3^{n+1}} \right),$$

where P is defined by

$$P_k^{(n)}(z) = \frac{1}{3} \left(-\beta_k^{(n)} + wz^2 + (1 - w + \beta_k^{(n)})z^3 + z^4 + (1 - w + \alpha_k^{(n)})z^5 + wz^6 - \alpha_k^{(n)}z^8 \right).$$

Analogously, two adjacent pairs of new level vertices in (9) can be reformulated by the following matrix form

$$[\lambda_{2k-1}^{(n+1)}, \lambda_{2k}^{(n+1)}, \lambda_{2k+1}^{(n+1)}, \lambda_{2k+2}^{(n+1)}] = [\lambda_{k-1}^{(n)}, \lambda_k^{(n)}, \lambda_{k+1}^{(n)}, \lambda_{k+2}^{(n)}] L_k^{(n)},$$

where the 4×4 square matrix $L_k^{(n)}$ is given by (15). The convergence behavior of schemes in (9) can be analyzed similarly. More precisely, we need to investigate the convergence behavior of the matrix product

$$\prod_{\ell=0}^n M_{3^\ell k}^{(\ell)} = L_k^{(0)} L_{2k}^{(1)} L_{2^2 k}^{(2)} \cdots L_{2^n k}^{(n)},$$

$$L_k^{(n)} = \begin{bmatrix} w & -\beta_k^{(n)} & 0 & 0 \\ 1-w+\alpha_k^{(n)} & 1-w+\beta_k^{(n)} & w & -\beta_{k+1}^{(n)} \\ -\alpha_k^{(n)} & w & 1-w+\alpha_{k+1}^{(n)} & 1-w+\beta_{k+1}^{(n)} \\ 0 & 0 & -\alpha_{k+1}^{(n)} & w \end{bmatrix}. \quad (15)$$

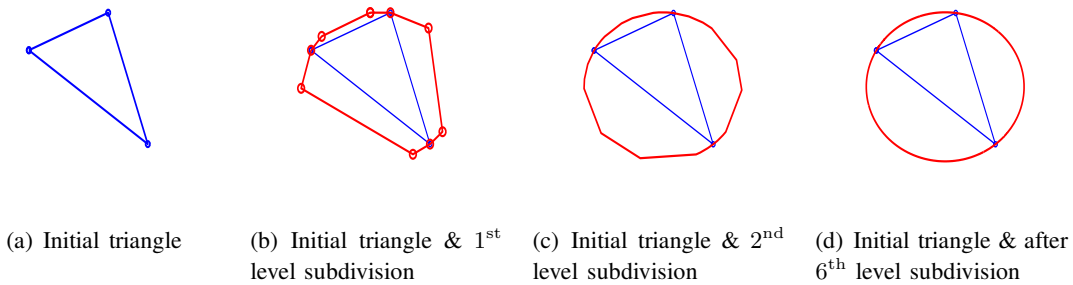


Figure 3. Ternary nonlinear interpolatory subdivision scheme in (6), with $w = 2/9$, is applied to an initial polygon as a triangle.

or the polynomial product

$$\prod_{\ell=0}^n Q_{2^\ell k}^{(\ell)} \left(e^{-i\omega/2^{n+1-\ell}} \right) = Q_{2^n k}^{(n)} \left(e^{-i\omega/2} \right) Q_{2^{n-1} k}^{(n-1)} \left(e^{-i\omega/2^2} \right) Q_{2^2 k}^{(1)} \left(e^{-i\omega/2^n} \right) Q_k^{(0)} \left(e^{-i\omega/2^{n+1}} \right),$$

where the polynomial Q is defined by

$$Q_k^{(n)}(z) = \frac{1}{2} \left(-\beta_k^{(n)} + wz + (1-w+\beta_k^{(n)})z^2 + (1-w+\alpha_k^{(n)})z^3 + wz^4 - \alpha_k^{(n)}z^5 \right).$$

Finally, the subdivision matrices for schemes in (13) can also be given by (15), with $\alpha_k^{(n)}$, $\alpha_k^{(n+1)}$, $\beta_k^{(n)}$ and $\beta_k^{(n+1)}$ replaced by $1/4 - w$. These matrices have eigenvalues 1, $1/2$, $1/4$, and $3/4 - 2w$. Therefore, they converge to continuous curves when $w \in (-1/8, 7/8)$; in at least a C^1 fashion when $w \in (1/8, 5/8)$; in at least C^2 when $w \in (1/4, 1/2)$. For $w = 5/16$, the associated refinable function is the quartic B -spline N_5 , so the scheme converges to a C^4 curve.

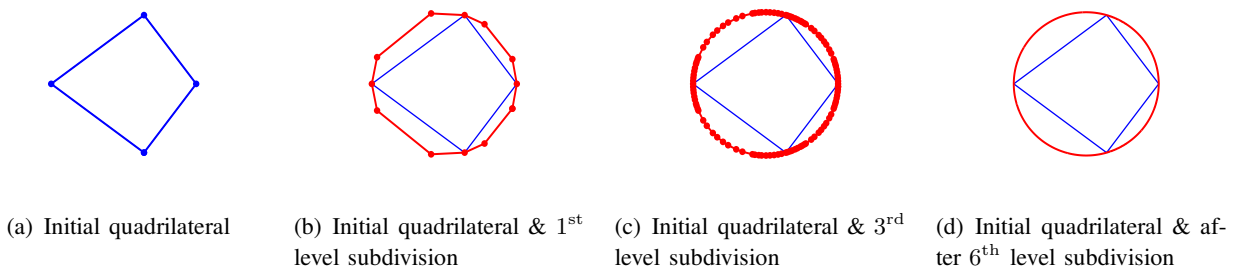


Figure 4. Ternary nonlinear interpolatory subdivision scheme in (6), with $w = 2/9$, is applied to an initial polygon as a quadrilateral.

4. Implementations

To show the elegance of our schemes, we will demonstrate the four families of schemes by applying them to mainly planar polygons.

4.1. Implementations of Nonlinear Ternary Interpolatory Schemes

We first implement our ternary interpolatory schemes to some simple polygons.

Fig. 3 shows the result with the initial polygon as a triangle. Fig. 4 shows the result with the initial polygon as a cyclic quadrilateral (with all its four vertices on a single circle). Not surprisingly, the limiting curves in both cases are the circumscribed circles of the triangle and cyclic quadrilateral.

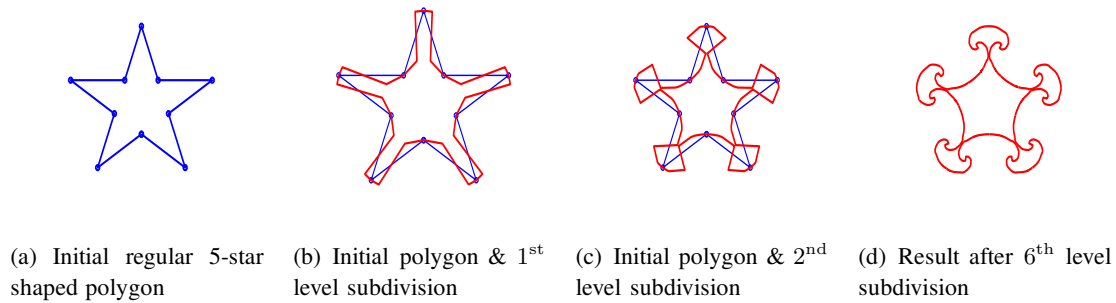


Figure 5. Ternary nonlinear interpolatory subdivision scheme in (6), with $w = 2/9$, is applied to an initial polygon as a regular 5-star shaped polygon.

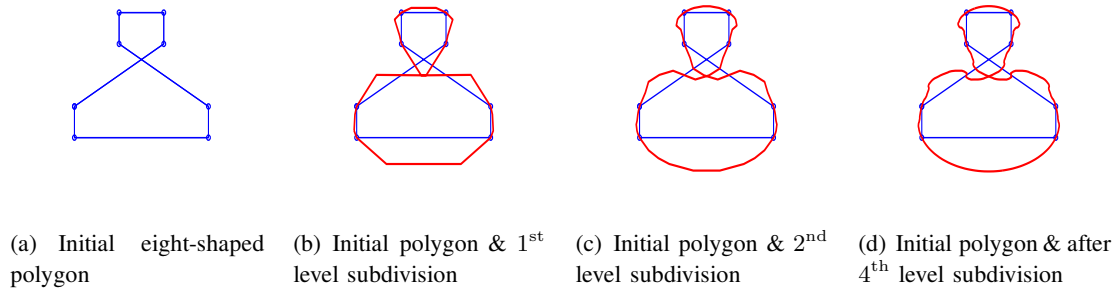


Figure 6. Ternary nonlinear interpolatory subdivision scheme in (6), with $w = 2/9$, is applied to an initial polygon as a eight-shaped polygon.

Fig. 5 shows the result with the initial polygon as a regular 5-star shaped polygon. Fig. 6 shows the result with the initial polygon as a eight-shaped polygon. These two figures show the behavior of the scheme for non-convex initial polygons.

4.2. Implementations of Nonlinear Binary Approximation Schemes

For comparison purpose, we first implement our corner-cutting binary approximation schemes to the triangle in Fig. 3(a). Fig. 7 shows the result with $w = 1/3$.

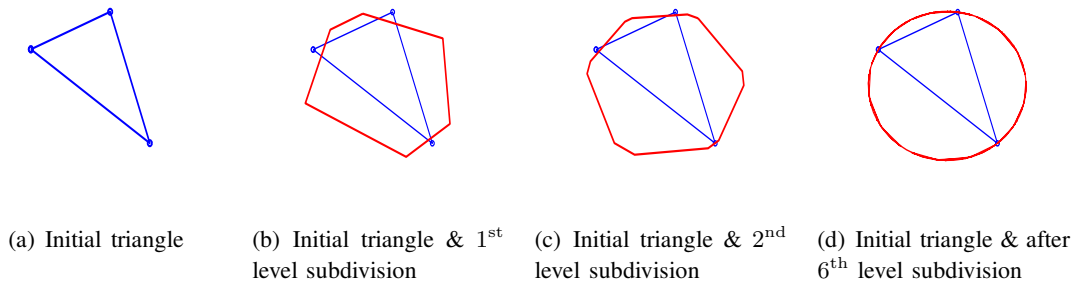


Figure 7. Binary nonlinear approximation subdivision scheme in (9), with $w = 1/3$, is applied to an initial triangle in Fig. 3(a).

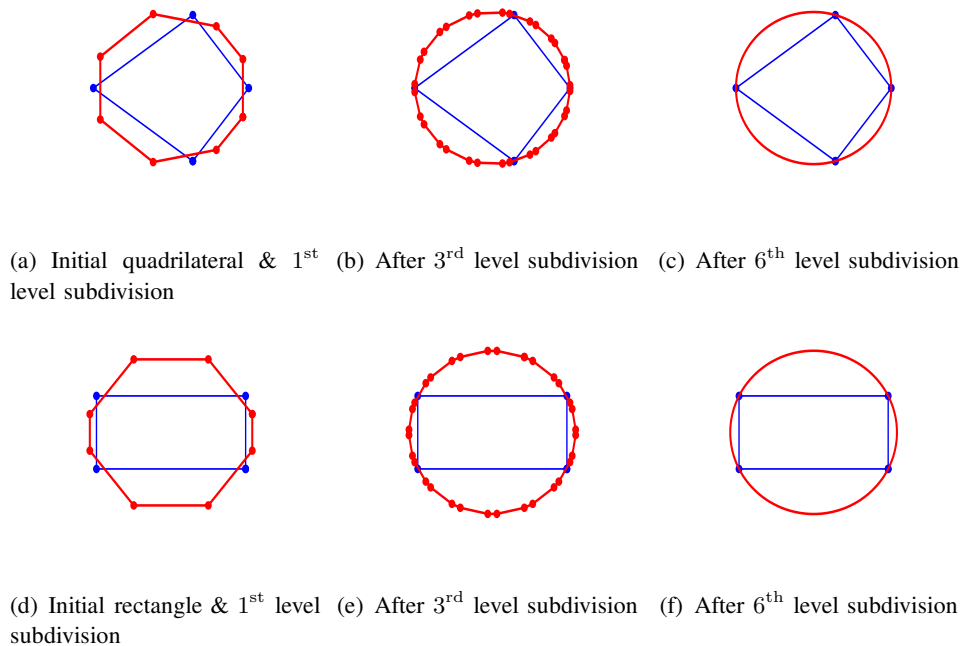


Figure 8. Binary nonlinear approximation subdivision scheme in (9), with $w = 1/4$, is applied to the quadrilateral in Fig. 4(a) and a rectangle.

Fig. 8(a)–8(c) shows the result with the initial polygon as the quadrilateral in Fig. 4(a). Fig. 8(d)–8(f) are results when the scheme is applied to a rectangle. Observe the corner-cutting behavior of our binary approximation schemes in both Fig. 8(a) and Fig. 8(d). Again, the limiting curves are the circumscribed circles of the quadrilaterals.

We end this section by pointing out that, similar to the choice for the tension parameter w in (1), some choices of w for both (6) and (9) will make the polygons themselves overlap.

4.3. Implementations of Both Linear Ternary Interpolatory and Linear Binary Corner-Cutting Schemes

In this section, we briefly demonstrate our 3-point linear ternary interpolatory schemes in (11)

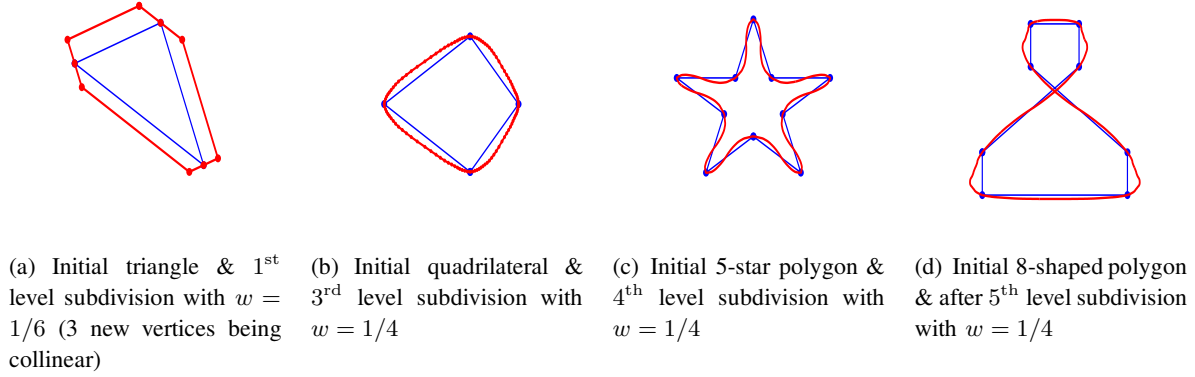


Figure 9. Linear ternary interpolatory subdivision schemes in (11), with $w = 1/6, 1/4, 1/4,$ and $1/4,$ respectively, are applied to the triangle in Fig. 3(a), the quadrilateral in Fig. 4(a), the 5-star polygon in Fig. 5(a), and the 8-shaped polygon in Fig. 6(a).

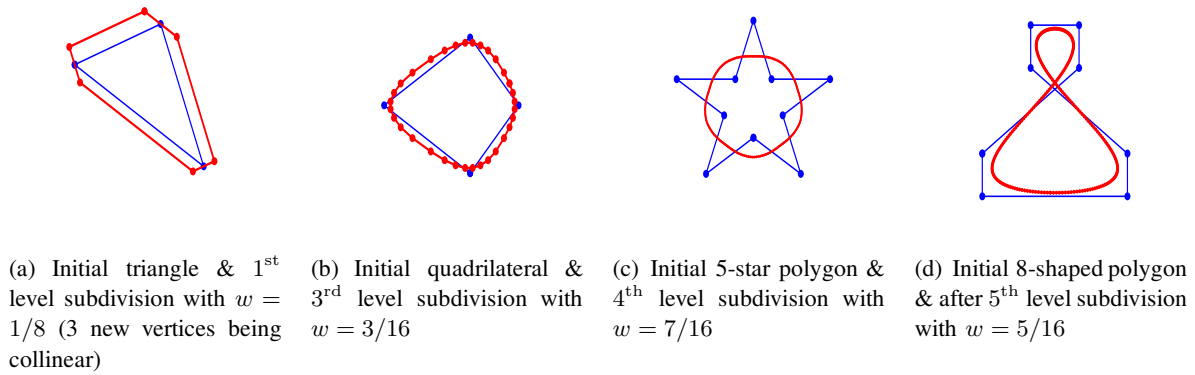


Figure 10. Corner-cutting binary linear approximation subdivision schemes in (12), with $w = 1/8, 3/16, 7/16,$ and $5/16,$ respectively, are applied to the triangle in Fig. 3(a), the quadrilateral in Fig. 4(a), the 5-star polygon in Fig. 5(a), and the 8-shaped polygon in Fig. 6(a).

and our 3-point linear, corner-cutting binary approximation schemes in (13).

Fig. 9 shows the results when (11) is applied to the triangle in Fig. 3(a) with $w = 1/6$, the quadrilateral in Fig. 4(a) with $w = 1/4$, the 5-star in Fig. 5(a) with $w = 1/4$, and the 8-shaped polygon in Fig. 6(a) with $w = 1/4$.

Fig. 10 shows the results when (13) is applied to the triangle in Fig. 3(a) with $w = 1/8$, the quadrilateral in Fig. 4(a) with $w = 3/16$, the 5-star in Fig. 5(a) with $w = 7/16$, and the 8-shaped polygon in Fig. 6(a) with $w = 5/16$ (quartic B -spline). Without going into details, the limiting curves have Hölder smoothness of $C^{.9062+\varepsilon}$, $C^{1.3076+\varepsilon}$, $C^{2.8597+\varepsilon}$, and C^4 , respectively, for some small $\varepsilon > 0$.

In addition, to summarize and demonstrate the implementation to 3D polygons, we apply our schemes to a 3D polygon that is formed from 6 edges and two diagonals of a cube, plotted progressively in Fig. 11(a). For comparison purposes, we have also included the graphs when the 4-point scheme is used.

5. Conclusion

Two new families of 3-point nonlinear subdivision schemes for curve design were established. The first family is ternary interpolatory and the second family is binary approximation. All of these new schemes are *circular-invariant*, meaning the limiting curves are circles when they are applied to cyclic polygons, such as triangles, squares, or rectangles. As consequences of both families, two new families of 3-point linear ternary interpolatory and binary approximation subdivision schemes were developed as well, where the latter is a naturally extension of the Lane-Riesenfeld schemes, which are corner-cutting depending on the choices of the tension parameter. The four families of schemes were implemented extensively by a variety of examples. Our future work will be three-fold: (1) to establish detailed smoothness analysis near vertices; (2) to develop “local adaptive” schemes for curve design; and (3) to incorporate the similar idea to developing efficient nonlinear subdivision schemes for surface design.

Acknowledgment

Research of the first author was partially supported by ARO under Grant W911NF-05-1-0388.

References

- [1] Chaikin, G. M. (1974). An algorithm for high speed curve generation. *Computer Vision, Graphics and Image Processing* **3**, 346–349.
- [2] Chui, C. K. and Lian, J.-A. (1995). Construction of compactly supported symmetric and antisymmetric orthonormal wavelets with scale = 3. *Appl. Comp. Harmonic Anal.* **2**, 21–51.
- [3] Daubechies, I., Orthonormal bases of compactly supported wavelets. *Comm. Pure & Appl. Math.* **41**, 909–996.
- [4] Doo, D. and Sabin, M. (1978). Behaviour of recursive division surfaces near extraordinary points. *Computer-Aided Design* **10**, 356–360.
- [5] Dyn, N., Levin, D., and Gregory, J. (1987). A 4-point interpolatory subdivision scheme for curve design. *Computer Aided Geometric Design* **4**, 257–268.
- [6] Hassan, M. F. and Dodgson, N. A. (2002). Ternary and three-point univariate subdivision schemes. In: *Curve and Surface Fitting: Saint-Malo 2002*, A. Cohen, J.-L. Merrien, and L. L. Schumaker (eds.), Nashboro Press, Brentwood, TN, 199–208.
- [7] Ivriissimtza, I. P., Dodgson, N. A., Hassan, M. F., and Sabin M. A. (2002). The refinability of the four point scheme. *Computer Aided Geometric Design* **19**, 235–238.
- [8] Lane, J. & Riesenfeld, R. (1980). A Theoretical Development for the Computer Generation and Display of Piecewise Polynomial Surfaces. *IEEE Transactions on Pattern Analysis and Machine Intelligence* **2**, 35–46.
- [9] Lian, J.-A. (2008). On a -ary subdivision for curve design: I. 4-point and 6-point interpolatory schemes. *Application & Applied Math.* **3**, 18–29.
- [10] Lian, J.-A. (2008). On a -ary subdivision for curve design: II. 3-point and 5-point interpolatory schemes. *Application & Applied Math.* **3**, 176–187.
- [11] de Rham, G. (1956). Sur une courbe plane. *Journal de Mathématiques Pures et Appliquées* **35**, 25–42.

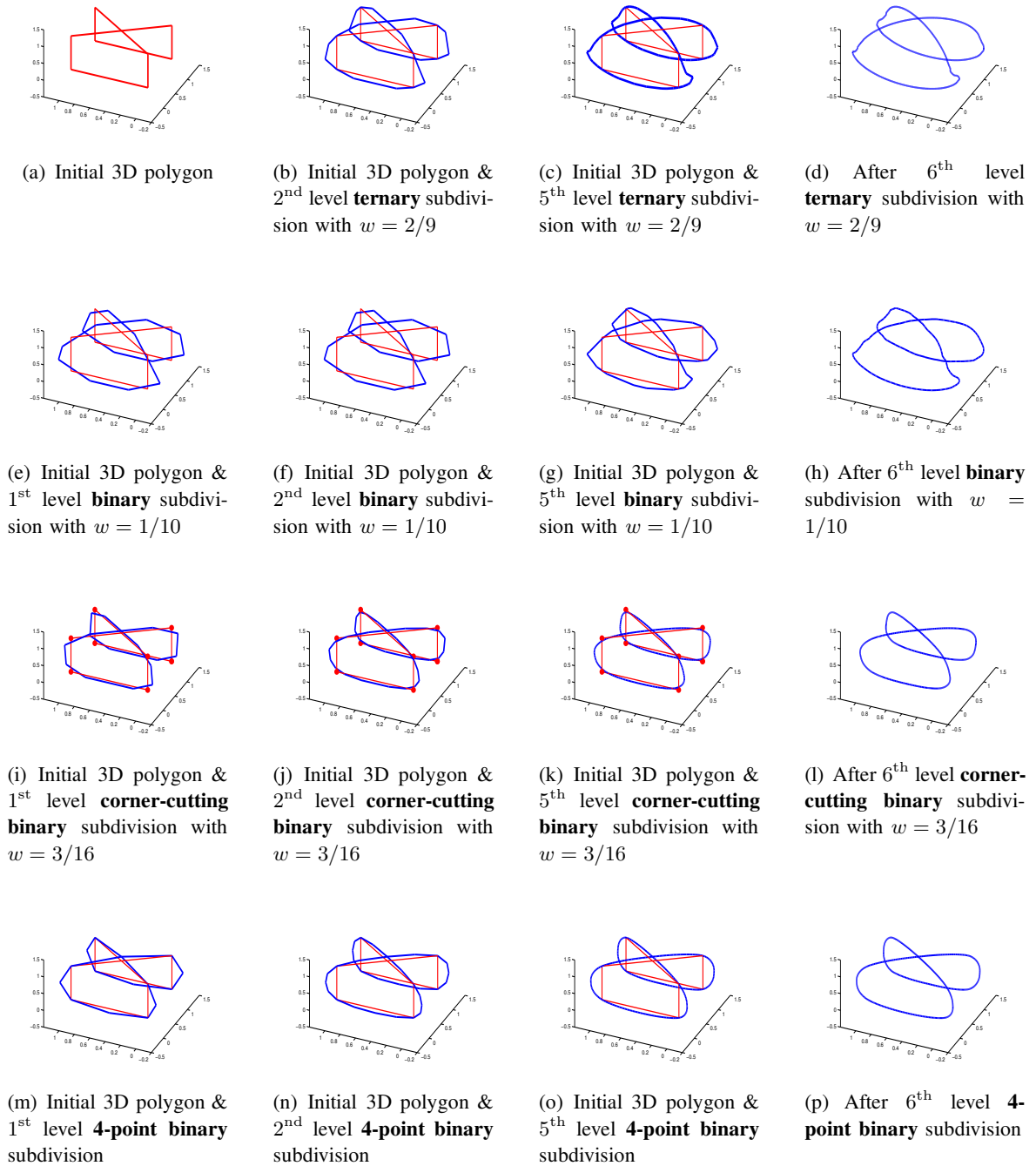


Figure 11. For comparison purposes, four schemes: nonlinear ternary interpolatory scheme, (a)–(d); binary approximation scheme with $w = 1/10$, (e)–(h); corner-cutting linear binary approximation scheme in (12) with $w = 7/16$, (i)–(l); and 4-point binary scheme, (m)–(p), are applied to a 3D polygon formed by 6 edges and 2 diagonals of a cube in Fig.11(a). The 6th-level subdivisions are given in Fig.11(d), Fig.11(h), Fig.11(l), and Fig.11(p), respectively.